

Research article

Application of Fractal modeling for mapping Hydrothermal Alteration Zones Using ASTER imagery in the southeastern part of IRAN

Mohammad Hossein Aghlan¹, Mohammad Hadi Hadigheh², Saeed Khojastehfar¹, Hojjatollah Ranjbar^{3*}

1- School Of Mining Engineering, College Of Engineering, University Of Tehran, Tehran, Iran

2- Kushamadan Consulting, Tehran, Iran

3- Dept. of Mining Engineering, Shahid Bahonar University of Kerman, Kerman, Iran

*Corresponding author: E-mail: h.ranjbar@uk.ac.ir

(Received: June 2025, Accepted: September 2025)

DOI: [10.22034/ANM.2025.23223.1683](https://doi.org/10.22034/ANM.2025.23223.1683)

Keywords	Abstract
Fractal modeling	This study presents an integrated approach to map hydrothermal argillic alteration zones using ASTER satellite imagery in the Jebal Barez region of southeastern Iran. The novelty of this research lies in the combination of Spectral Angle Mapper (SAM), Matched Filtering (MF), and fractal value-area modeling for anomaly detection and classification. After atmospheric correction using the IARR method, kaolinite spectral signatures were extracted and used in the SAM and MF techniques to delineate altered zones. A total of 34 ground control points were collected across representative lithologies to validate remote sensing outputs. SAM and MF both identified key alteration zones, with MF demonstrating higher classification accuracy (82.35%) compared to SAM (73.52%). The fractal model enabled effective separation of anomalous zones by detecting scale-invariant spatial patterns and extracting critical breakpoints. The integration of fractal modeling with spectral analysis provided improved anomaly delineation and exploration targeting. Field validation confirmed the presence of Pb-Zn mineralization and silica-rich alteration in high-response zones. This methodology offers a replicable framework for mineral exploration in complex terrains using freely available remote sensing data. A detailed workflow chart is also proposed to enhance clarity and reproducibility.
Anomaly detection	
Remote sensing	
Hydrothermal alteration	
ASTER imagery	
Argillic zone	
Jebal Barez	

1. INTRODUCTION

The concept of fractals, introduced by Mandelbrot in the 1980s, describes self-similar patterns that remain consistent across different scales. Fractal geometry enables the analysis of complex natural shapes beyond the scope of classical Euclidean geometry [1]. Building on this, multifractals describe systems governed by a multifractal spectrum [2–6] and are widely applied to scale-invariant phenomena [7].

Numerous geological processes—such as mineralization, sedimentation, volcanism, and

landform evolution—exhibit self-similarity and are well-modeled using fractal and multifractal approaches [6, 8–9], making fractal analysis a valuable tool in geoscience [10–11]. In mineral exploration, fractal-based techniques (e.g., box-counting, number-size, radial density, concentration-area (C-A), concentration-distance (C-D), and local singularity models) help delineate geochemical and geophysical anomalies while preserving key spatial and statistical properties [12–21].

In remote sensing, spectral classifiers such as the Spectral Angle Mapper (SAM) are widely used

to identify alteration minerals associated with mineralization by comparing pixel spectra to known reference spectra [22–24]. Similarly, the Matched Filter (MF) method enhances mineral mapping by maximizing the signal-to-noise ratio with respect to specific spectral endmembers [25–26].

This study focuses on the identification and delineation of hydrothermal alteration zones in a part of southeastern Iran, specifically within the Jebal Barez region. ASTER satellite imagery was utilized in combination with two widely recognized spectral analysis methods: the Spectral Angle Mapper (SAM) and Matched Filter (MF). These techniques were applied to detect argillic alteration zones indicative of potential mineralization. To enhance the interpretation and spatial characterization of alteration intensity, the results were further analyzed using the value-area fractal model, which enables quantitative classification and prioritization of alteration zones for mineral exploration purposes. Despite the proven utility of spectral methods in alteration mapping, the integration of fractal models for enhancing spatial analysis and anomaly detection remains underexplored, particularly in the Jebal Barez region. This study aims to fill this gap by applying a value-area fractal approach to quantify alteration intensity derived from ASTER-based spectral classification, thereby improving mineral target delineation. The main objective is to integrate SAM and MF outputs with fractal

modeling to enhance spatial analysis of alteration zones and validate results through field sampling and petrographic studies.

2. STUDY AREA

The study area is located in southern Kerman Province, Iran, approximately 45 km northeast of the city of Jiroft, between $57^{\circ}58'36''$ – $58^{\circ}04'07''$ E and $28^{\circ}44'32''$ – $28^{\circ}49'09''$ N (Fig. 1). It lies within the southeastern segment of the Urmia–Dokhtar magmatic arc, a subduction-related belt formed by the convergence of the Arabian and Iranian plates. This magmatic arc, comparable to Andean-type systems, is composed of extensive volcanic and intrusive rocks [27–30].

The regional geology includes two primary lithological units:

- The Ert unit, consisting of volcanic and pyroclastic rocks such as rhyolitic pyroclasts, basaltic andesites, and agglomerates, is predominantly observed in the northern part of the study area.
- The Gd unit comprises granitic to quartz dioritic intrusive rocks that have intruded into Eocene formations across the northern and southern regions.

Additionally, dyke-like intrusions (unit d), ranging from diorite to quartz diorite in composition, crosscut the older units and are typically concentrated around major intrusive bodies (Fig. 2).

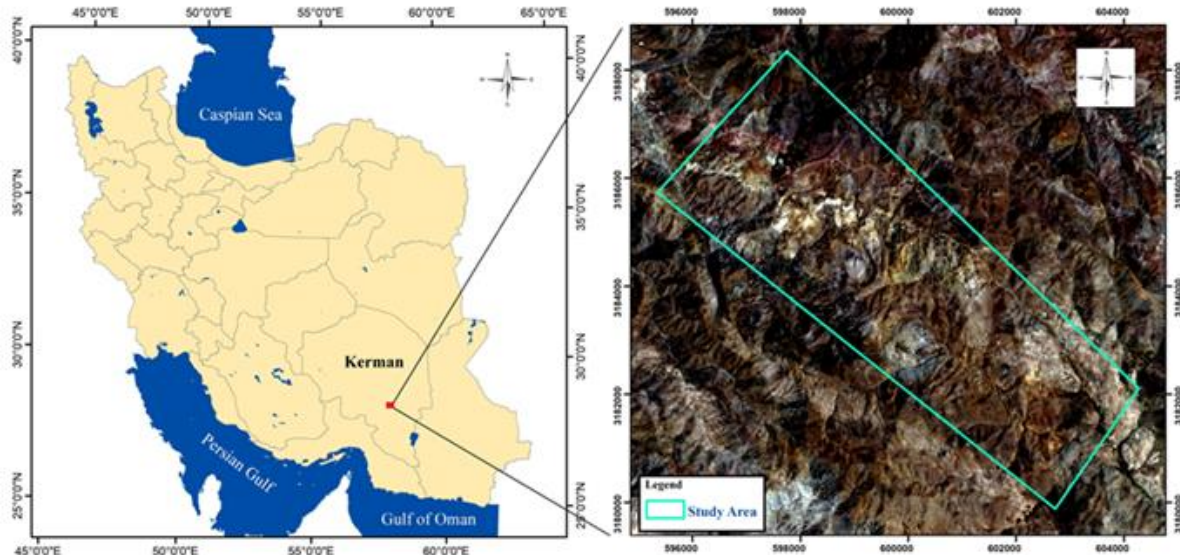


Fig.1. Geographical location and access routes of the study area.

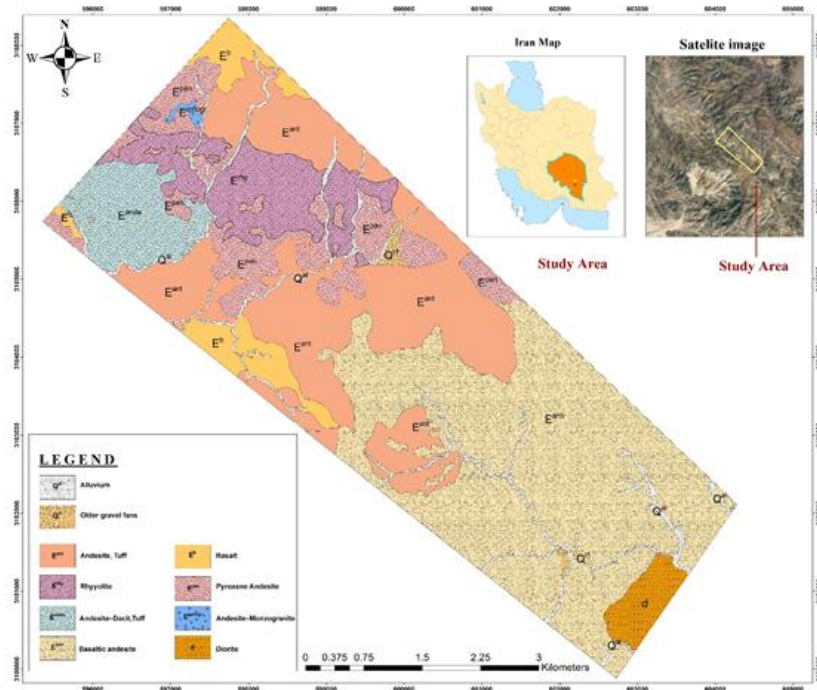


Fig. 2. The case study is located in the southeast of Urmia-Dokhtar volcanic belt and the Kerman copper.

From an economic perspective, the region hosts lead-zinc mineralized veins rich in chalcopyrite, sphalerite, and galena. These veins occur primarily within andesitic and pyroclastic rocks and are structurally controlled, often associated with iron oxide mineralization—indicative of hydrothermal processes and a favorable environment for mineral exploration.

3. DATA AND METHODS

The Advanced Spaceborne Thermal Emission and Reflection Radiometer (ASTER) is a multispectral imaging sensor widely utilized in geological applications. It provides 14 spectral bands across three subsystems: VNIR (3 bands, 15 m), SWIR (6 bands, 30 m), and TIR (5 bands, 90 m). This study employed Level 1T (L1T) ASTER imagery (scene AST_L1T_00306172007065639, acquired on June 17, 2007), pre-processed with radiometric, geometric, and topographic corrections. Atmospheric correction was applied using the Internal Average Relative Reflectance (IARR) method.

Additionally, ASTER is equipped with a backward-looking VNIR telescope that provides 15 m stereo imagery [31]. This study utilized Level 1T (L1T) ASTER imagery, which includes radiometric, geometric, and terrain corrections. The specific scene analyzed was AST_L1T_00306172007065639, acquired on June 17, 2007.

Radiometric correction was conducted using the IARR (Internal Average Relative Reflectance) method within ENVI software. This technique normalizes image spectra by internal averaging, minimizing the impact of atmospheric and topographic effects — especially important in arid, high-relief regions like southeastern Iran.

To investigate the spectral characteristics of alteration minerals, field samples were collected and analyzed. The spectral signatures of kaolinite—an indicator of argillic alteration—were extracted for use in the Spectral Angle Mapper (SAM) and Matched Filtering (MF) techniques. Following alteration mapping, a fractal-based analysis was applied to separate anomalous zones from the geologic background. Ground validation was performed through field observations and sample analysis to assess the accuracy of classification results for both SAM and MF. Atmospheric correction was conducted prior to processing using the Internal Average Relative Reflectance (IARR) method.

3.1. Spectral Characteristics Of Argillic Alteration

Kaolinite, a principal indicator of argillic alteration, exhibits distinct absorption features in the SWIR region. These include a strong absorption band near $2.2\text{ }\mu\text{m}$ and a weaker one at $2.15\text{ }\mu\text{m}$, both associated with Al-OH vibrations. A notable absorption around $1.4\text{ }\mu\text{m}$ is also linked to OH-stretching modes [32] (Fig. 3).

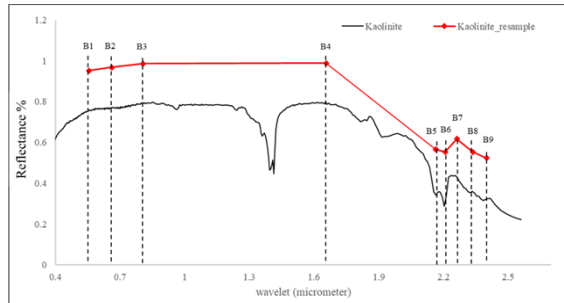


Fig. 3. Spectral profile of kaolinite (0.4–2.5 μm) with resampled bands corresponding to ASTER sensor wavelengths (adapted from USGS spectral library).

3.2. Alteration Mapping Using Spectral Angle Mapper (SAM)

The Spectral Angle Mapper (SAM) is a widely adopted technique in remote sensing for mineral exploration [33–34]. It quantifies spectral similarity by calculating the angle between a target pixel's spectrum and a reference spectrum in n-dimensional space. Both spectra are treated as vectors, and their angular relationship is measured using the following formula:

$$\cos \alpha = \frac{\sum_{i=1}^{nb} t_i \cdot r_i}{\sum_{i=1}^{nb} t_i^2 \cdot \sum_{i=1}^{nb} r_i^2} \quad (1)$$

where t_i and r_i are the reflectance values of the target and reference spectra in band i . SAM produces two outputs: a rule image showing the spectral angle for each pixel (lower angles = better match), and a classification image based on user-defined thresholds.

3.3. Alteration Mapping Using Matched Filtering (MF)

The Matched Filtering (MF) method is used to estimate the presence of specific target endmembers in mixed pixels [35]. It enhances the spectral response of the target while suppressing background noise, effectively maximizing the signal-to-noise ratio.

MF generates fraction images for each target endmember, with grayscale pixel values ranging from 0 to 1—where 1 represents a perfect spectral match, and 0 indicates no similarity [36–37].

3.4. Rationale For Method Selection And Modeling Strategy

SAM and MF were selected due to their proven effectiveness in identifying hydroxyl-bearing alteration minerals such as kaolinite and alunite[38–39]. SAM measures spectral similarity by calculating the angle between image and reference spectra, while MF enhances the target spectral response by suppressing background interference.

In this study, kaolinite spectra from the USGS spectral library were resampled to match ASTER bands and used as reference. For SAM, classification thresholds were empirically set at 0.1 radians after trial runs to minimize false positives. MF outputs were thresholded using statistical cutoffs derived from histogram analysis of fraction images (mean + 1.5σ).

Following spectral classification, the fractal value-area model was applied to quantify the spatial distribution of alteration intensities. This model plots the cumulative area above a given pixel value versus the pixel value itself on a log-log scale, revealing linear segments that correspond to distinct geospatial regimes. Breakpoints in these plots were determined visually and statistically using slope-change detection, and used to classify pixels into background, weak, and strong anomalies.

The MF and SAM grayscale outputs served as input images for fractal modeling, enabling a hierarchical classification based on spatial complexity. This integration improved the identification of discrete alteration zones and supported prioritization of field validation targets.

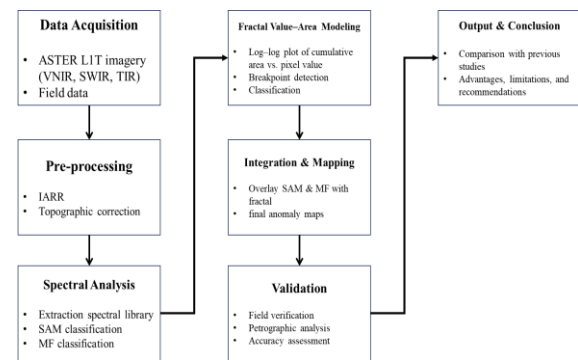


Fig. 4. Workflow of the research methodology applied in this study.

4. RESULTS AND DISCUSSION

To assess the performance of the SAM and MF techniques, spectral match outputs were thresholded based on histogram analyses. For SAM, an angular threshold of 0.1 radians was applied to highlight areas of strong spectral similarity with kaolinite. For MF, pixel values above 0.45 (mean + 1.5σ) were considered indicative of probable alteration. Visual comparison between Figures 5a and 5b reveals broader coverage by SAM, identifying generalized alteration halos, whereas MF shows higher spatial contrast and more localized high-intensity zones. This difference reflects SAM's sensitivity to broad spectral features and MF's ability to suppress background noise and highlight pure endmembers. The SAM and MF techniques were

implemented using reference spectra from the United States Geological Survey (USGS) spectral library. Both methods successfully identified hydrothermal alteration zones, which were subsequently verified through field observations.

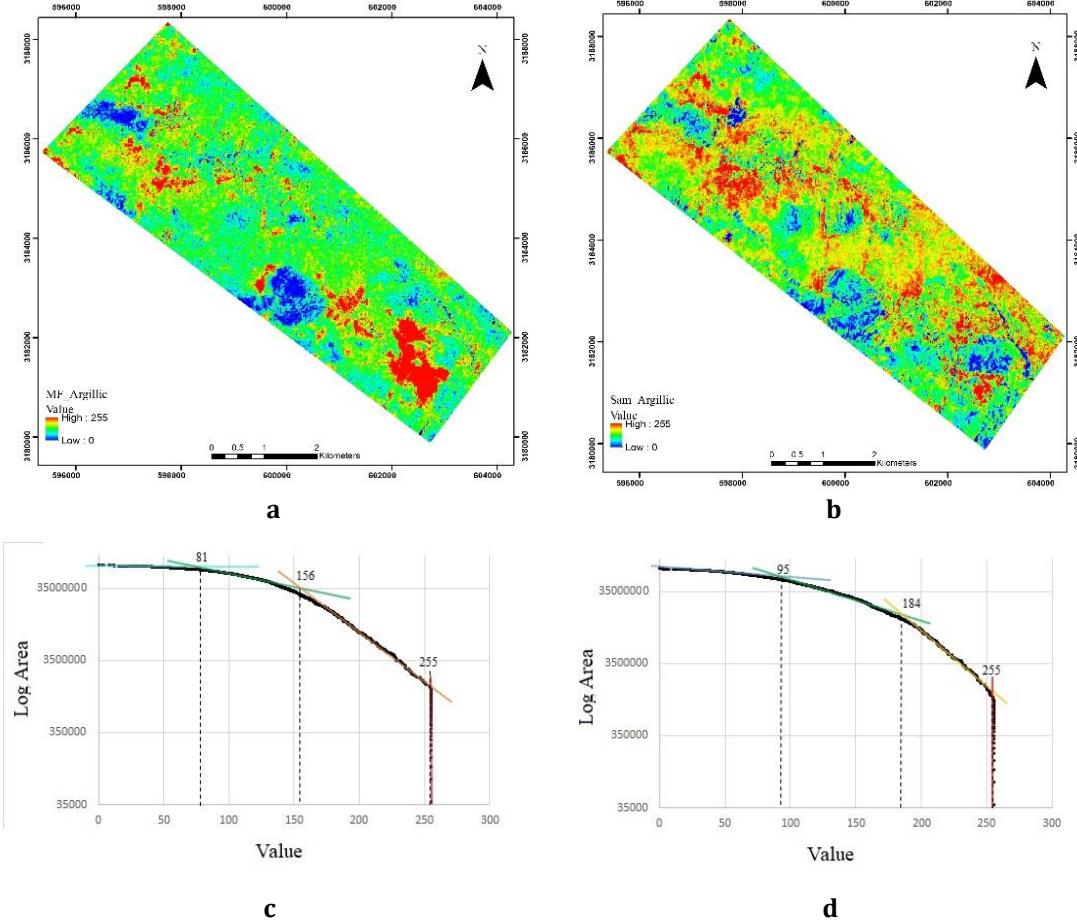


Fig. 5. (a) Argillic alteration zones derived from Matched Filtering (MF). (b) Argillic alteration zones mapped using the Spectral Angle Mapper (SAM). (c) Value-area fractal plots for MF and (d) SAM outputs.

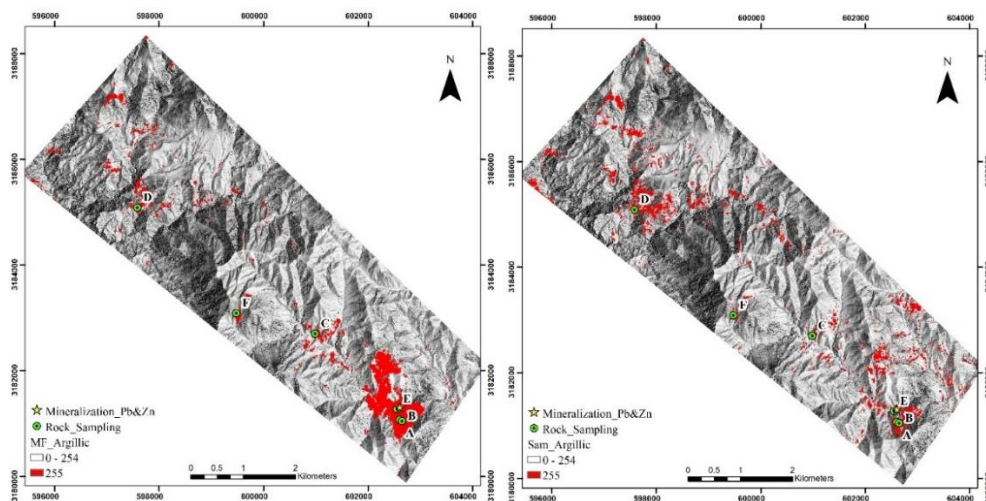


Fig. 6. Detailed field photographs and petrographic views of six representative ground control points (GCPs) selected from the total set of 34 samples. These samples were chosen to reflect a variety of lithologies and alteration intensities. Overlay of alteration zones (value = 255) from (a) MF and (b) SAM techniques with field data including sampling sites and Pb-Zn mineral occurrences.

Field investigations confirmed that mineralization in these altered zones primarily occurs as siliceous veins enriched in lead and zinc, with galena and sphalerite identified as the main ore minerals. As shown in Figures 5a and 5b, both MF and SAM successfully delineated argillic alteration zones, with the MF technique offering more localized and high-contrast outputs. The fractal value-area plots in Figure 5c confirm the presence of scale-invariant patterns within the mapped data. Identified breakpoints at values 81 and 156 (MF), and 95 and 184 (SAM), effectively separate background from anomalous regions. Figure 6 demonstrates strong spatial agreement between high-response alteration zones (red pixels) and field-verified Pb-Zn mineralization sites, particularly in the southern sector. Sampling points coincide with MF and SAM anomalies, validating the spectral results.

Fractal value-area plots were generated by ranking pixel values and plotting cumulative area versus value on a log-log scale. Breakpoints were identified visually and numerically as inflection points where slope changes occur, indicating transitions between background and anomaly regimes.

For MF (Figure 5c), breakpoints at pixel values 81 and 156 effectively delineated low-, medium-, and high-intensity alteration. Similarly, SAM-derived values at 95 and 184 (Figure 5d) reflect consistent spatial trends. These thresholds were subsequently used to reclassify output maps for interpretation.

The findings are consistent with previous studies in Iran and other regions with similar geological settings. For instance, Tangestani et al. (2008) reported effective alteration mapping using ASTER in the Shahr-e-Babak region, but without employing fractal analysis. Similarly, Afzal et al. (2011) applied C-A fractal models for porphyry Cu systems but relied on geochemical data. Our integration of SAM/MF with value-area fractal modeling represents a novel contribution by enabling anomaly separation directly from remote sensing outputs, offering both spatial precision and scalability.

Compared with previous ASTER-based alteration mapping in SE Iran (e.g., Tangestani et al., 2008) and fractal applications primarily in geochemical domains (e.g., Afzal et al., 2011), our approach integrates fractal value-area analysis directly with SAM/MF outputs. This yields objective, reproducible thresholds for anomaly separation and improves target prioritization without requiring additional ancillary datasets.

Petrographic observations (sericitic/argillic overprint, iron-oxide veining, silica enrichment)

are consistent with SWIR absorption features detected for kaolinite-bearing alteration, supporting both SAM halos and MF high-contrast centers. The spatial coincidence between mapped high-value pixels and hand-specimen/mineralogical evidence strengthens the interpretation of argillic alteration zones as validated targets.

5. ACCURACY ASSESSMENT

In this study, a total of 34 ground control points (GCPs) were collected across different lithologies and alteration zones for validation. Six representative samples (Fig. 6) were selected for detailed petrographic and spectral examination because they cover the range of alteration intensities and lithological contexts observed in the field. The locations of all 34 GCPs are shown in Figure 7. This approach allows in-depth discussion of typical alteration patterns while ensuring that the accuracy assessment incorporates the full validation set.

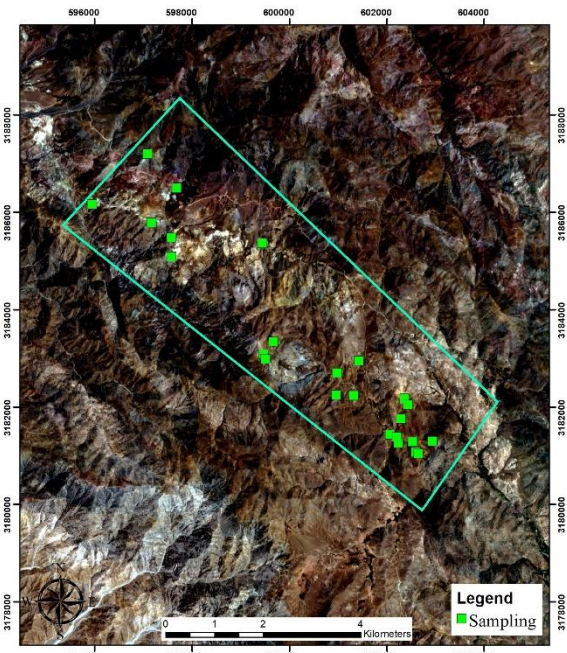


Fig. 7. Spatial distribution of ground control sampling points within the study area.

To validate the remote sensing results, a field survey was conducted to verify zones of argillic alteration, iron oxide staining, and kaolinite occurrences visually identified in ASTER imagery. Ground-truth observations were used to assess the performance of the SAM and MF classification methods by comparing pixel-based predictions with field data (Figures 8 and 9). The Matched Filtering (MF) method achieved an overall classification accuracy of 82.35%, while the Spectral Angle Mapper (SAM) achieved 73.52%

accuracy, as presented in Table 1. The classification accuracy was assessed by comparing remote sensing outputs (SAM and MF) to field-verified control points. Confusion matrices were constructed, and overall accuracy was calculated. The MF method yielded 82.35% accuracy (28/34 correct predictions), while SAM achieved 73.52% (25/34). These results indicate higher spatial precision for MF in mapping argillic alteration. The observed misclassifications were primarily in transitional zones, suggesting potential spectral mixing or sub-pixel heterogeneity. Further field validation involved petrographic analysis of representative rock samples collected from selected alteration zones. Two key samples are described below:

To further validate the alteration zones identified through remote sensing, selected rock samples were prepared as thin sections and analyzed under a polarizing microscope. Two representative samples are described below, highlighting key mineralogical features and hydrothermal alteration signatures. Figure 8 highlights a significant variation in the spatial distribution of alteration zones derived from SAM and MF. MF (Fig. 8a) isolates more compact and

high-contrast alteration centers, while SAM (Fig. 8b) maps broader and less distinct halos. These differences emphasize MF's higher specificity and SAM's broader sensitivity. This complementarity suggests the potential benefit of integrating both outputs in a hybrid decision-support system for exploration.

Petrographic analysis confirmed the presence of alteration minerals such as sericite, epidote, and kaolinite in samples collected from mapped anomalous zones. These minerals correspond with absorption features detected in the SWIR bands of ASTER, validating the spectral approach. The spatial overlap between altered outcrops and high-value pixels in MF and SAM maps supports the robustness of the classification framework. Some limitations affect the accuracy assessment. First, field sampling was constrained by terrain accessibility, potentially biasing spatial coverage. Second, spectral confusion due to overlapping mineral features may result in classification errors. Third, weathering effects and vegetation may obscure alteration signatures in some zones. These factors should be considered when extrapolating results to broader regions.

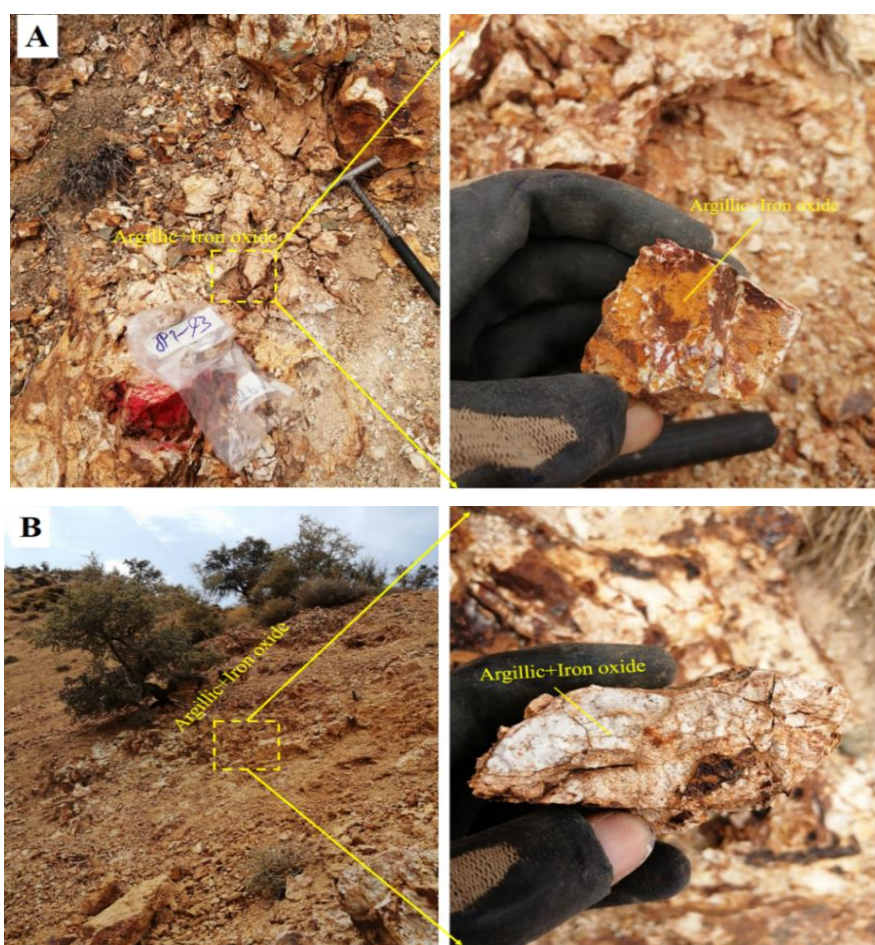


Fig. 8. (A, B) Outcrops of argillic alteration observed in dioritic and granodioritic rocks in the southeastern part of the study area.

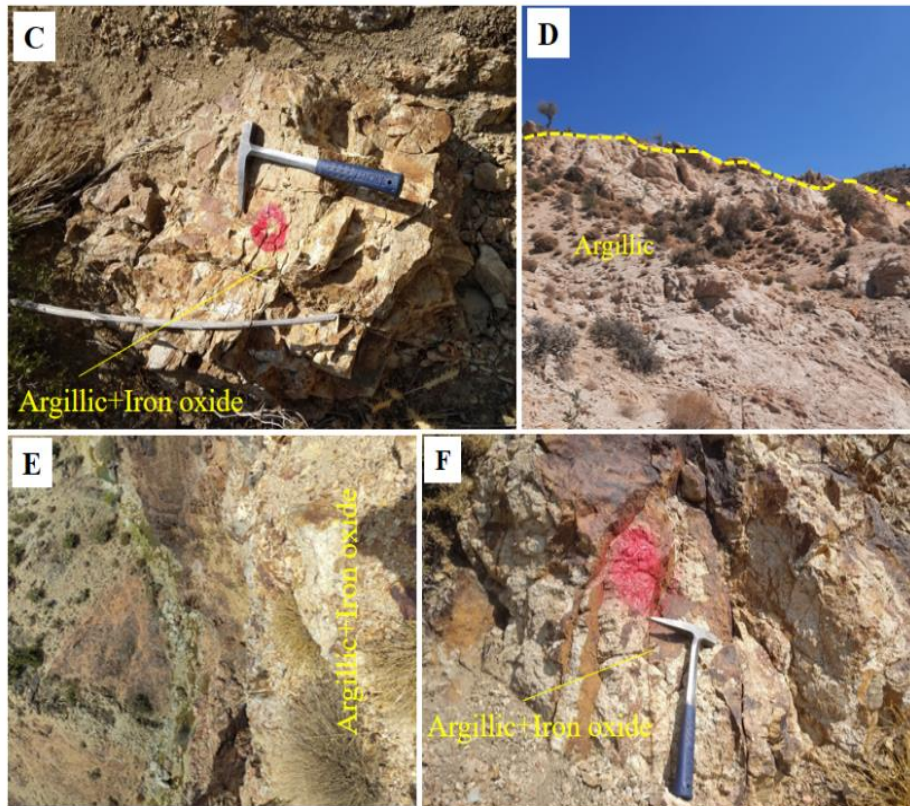


Fig. 9. (C, D) Iron oxide vein networks formed within argillic alteration units, with vein thicknesses ranging from 1 to 10 cm. (E) Iron oxide outcrop in andesitic rocks located in the northern to central parts of the study area. (F) Argillic alteration outcrop observed in diorite, located in the central sector.



Fig. 10. Silica-rich veins with visible galena and Pb-Zn mineralization in the northern part of the study area, providing ground evidence in support of remote sensing results.

Table 1. The overall accuracy for SAM and MF methods in detecting hydrothermal alterations

Method MF		Method SAM	
Predict	class	Predict	class
Other	6	Other	9
Argillic	28	Argillic	25
total	34	total	34
Accuracy Assessment%	82.35	Accuracy Assessment%	73.52

To further validate the alteration zones identified through remote sensing, selected rock samples were prepared as thin sections and analyzed under a polarizing microscope. Two representative samples are described below, highlighting key mineralogical features and hydrothermal alteration signatures.

5.1. Sample 1: Altered And Silicified Quartz-Monzogranite

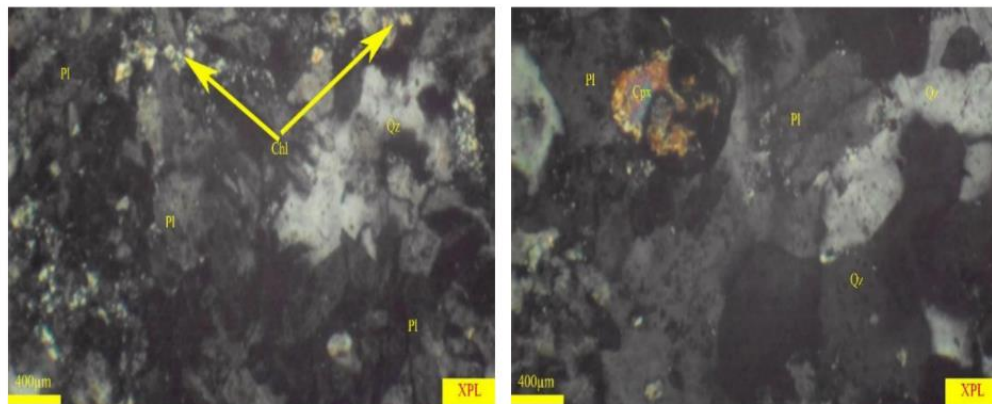


Fig. 11. Photomicrograph of Sample 1 showing altered plagioclase (sericitic and argillic), subhedral quartz, and pyroxene grains with evidence of iron oxide overprint.

5.2. Sample 2: Altered Volcanic Rock

This sample is interpreted as an altered intrusive volcanic unit with porphyritic to massive texture. The rock has undergone significant hydrothermal overprinting, characterized by sericitic, argillic, and local epidotic alteration.

Plagioclase: The dominant phase, appearing as subhedral crystals (>1 mm), moderately to intensely altered by sericite and clay minerals.

This sample exhibits a poikilitic texture and intense hydrothermal alteration. The mineral assemblage includes sericitic, argillic, epidotic, and phyllitic alteration types, indicative of prolonged fluid-rock interaction. Major mineral components include quartz, alkali feldspar, and plagioclase.

Plagioclase (~35%): Euhedral to subhedral tabular crystals (0.5–1.5 mm), extensively altered to sericite, clay minerals, epidote, and other phyllosilicates.

Quartz (~15%): Subhedral grains approximately 1 mm in size.

Alkali feldspar (~25%): Strongly altered to sericite and clay; crystal size ranges from 0.3 mm to >1 mm.

Pyroxene (<10%): Occurs as scattered subhedral grains (<1 mm), often associated with iron oxide

Epidote: Present in localized zones, suggesting multiphase fluid evolution.

Quartz and alkali feldspar (~35%): Subhedral grains ranging from 0.3 mm to >1 mm.

Siliceous veining: Composed of subhedral quartz, cross-cutting the matrix and indicative of late-stage silica mobilization.

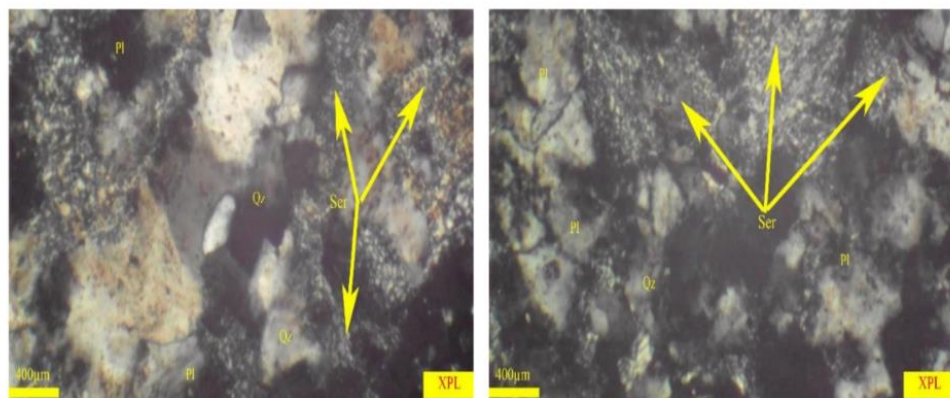


Fig. 12. Photomicrograph of Sample 2 showing altered plagioclase (sericitic and argillic), semi-formed quartz crystals, and quartz-rich veinlets.

6. SUMMARY AND CONCLUSIONS

This study successfully delineated hydrothermal argillic alteration zones in the Jebal Barez region through an integrated approach combining ASTER satellite imagery, spectral classification (SAM and MF), and fractal value-area modeling.

SAM and MF both identified key altered zones, with MF achieving a higher accuracy (82.35%) in pixel-level classification compared to SAM (73.52%). Fractal modeling revealed scale-invariant spatial patterns and allowed threshold-based classification of anomalies, improving the interpretation of alteration intensity.

Field validation, including petrographic analysis of representative samples, confirmed the presence of kaolinite, iron oxides, and Pb-Zn mineralization in high-response areas. The strong spatial correlation between mapped anomalies and ground evidence underscores the effectiveness of the integrated methodology.

While SAM offered broader coverage of alteration halos, MF provided greater sensitivity to pure mineral signatures. Their combined use enhances both detection and spatial refinement of anomalies. Despite the promising results, certain limitations remain. ASTER's moderate spatial resolution may limit the detection of small or narrow alteration features. The fractal model relies on empirical breakpoint selection, which may introduce subjectivity. Future research should explore integration with hyperspectral data and machine learning-based anomaly detection to enhance predictive performance and reduce uncertainty.

Acknowledgment

The authors would like to express their sincere gratitude to the Geological Survey Organization for providing essential datasets that supported the

execution of this research. Appreciation is also extended to Kusha Madan Consulting Engineers for their logistical support and for making additional data and resources available throughout the course of the study.

REFERENCES

- [1] Davis, J. C. (2002). Statistics and data analysis in Geology (3rd ed.) (pp. 342–353). New York: Wiley.
- [2] Feder, J. (1988). Fractals New York: Plenum.
- [3] Stanley, H., & Meakin, P. (1988). Multifractal phenomena in physics and chemistry. *Nature*, 335(6189), 405–409.
- [4] Evertz, C. J. G., & Mandelbrot, B. B. (1992). Multifractal measures. Appendix B. In H.-O. Peitgen, H. Jurgens, & D. Saupe (Eds.), *Chaos and fractals* (pp. 922–953). New York: Springer.
- [5] Agterberg, F. P., Cheng, Q., & Wright, D. F. (1993). Fractal modelling of mineral deposits. In J. Elbrond & X. Tang (Eds.), *Application of computers and operations research in the mineral industry* (pp. 43–53). Proceedings of the 24th APCOM Symposium. Montreal: Canadian Institute of Mining Metallurgy and Petroleum.
- [6] Cheng, Q. (1994). Multifractal modeling and spatial analysis with GIS: Gold potential estimation in the Mitchell-Sulphurets area, northwestern British Columbia. Unpublished Doctoral Dissertation, School of Graduate Studies and Research, University of Ottawa.
- [7] Mandelbrot, B. B. (1974). Intermittent turbulence in self-similar cascades: Divergence of high moments and dimension of the carrier. *Journal of Fluid Mechanics*, 62(2), 331–358.
- [8] Cheng, Q., Bonham-Carter, G. F., Hall, G. E. M., & Bajc, A. (1997). Statistical study of trace elements in the soluble organic and amorphous Fe–Mn phases of surficial sediments, Sudbury Basin, 1, Multivariate and spatial analysis. *Journal of Geochemical Exploration*, 59(1), 27–46.

[9] Cheng, Q. (1999b). Multifractality and spatial statistics. *Computers & Geosciences*, 25(9), 949–961.

[10] Panahi, A., Cheng, Q., & Bonham-Carter, G. F. (2004). Modeling lake sediment geochemical distribution using principal component, indicator kriging and multifractal power-spectrum analysis: a case study from Gowganda, Ontario. *Geochemistry: Exploration, Environment, Analysis*, 4(1), 59–70.

[11] Zuo, R., & Xia, Q. (2009). Application fractal and multifractal methods to mapping prospectivity for metamorphosed sedimentary iron deposits using stream sediment geochemical data in eastern Hebei province, China. *Geochimica et Cosmochimica Acta*, 73, A1540.

[12] Deng, J., Fang, Y., Yang, L. Q., Yang, J. C., Sun, Z. S., Wang, J. P., et al. (2001). Numerical modelling of ore-forming dynamics of fractal dispersive fluid systems. *Acta Geologica Sinica*, 75(2), 220–232.

[13] Deng, J., Wang, Q. F., Huang, D. H., Wan, L., Yang, L. Q., & Gao, B. F. (2006). Transport network and flow mechanism of shallow ore-bearing magma in Tongling ore cluster area. *Science in China (Series D)*, 49(4), 397–407.

[14] Mandelbrot, B. B. (1983). *The fractal geometry of nature (updated and augmented)*. New York: Freeman.

[15] Turcotte, D. L. (2002). Fractals in petrology. *Lithos*, 65(3–4), 261–271.

[16] Wang, Q. F., Deng, J., Liu, H., Yang, L. Q., Wan, L., & Zhang, R. Z. (2010). Fractal models for ore reserve estimation. *Ore Geology Reviews*, 37(1), 2–14.

[17] Raines, G. L. (2008). Are fractal dimensions of the spatial distribution of mineral deposits meaningful? *Natural Resources Research*, 17, 87–97.

[18] Carranza, E. J. M., Owusu, E., & Hale, M. (2009). Mapping of prospectivity and estimation of number of undiscovered prospects for lode-gold, southwestern Ashanti Belt, Ghana. *Mineralium Deposita*, 44(8), 915–938.

[19] Li, C. J., Ma, T. H., & Shi, J. F. (2003). Application of a fractal method relating concentration and distances for separation of geochemical anomalies from background. *Journal of Geochemical Exploration*, 77(2), 167–175.

[20] Cheng, Q., Agterberg, F. P., & Ballantyne, S. B. (1994). The separation of geochemical anomalies from background by fractal methods. *Journal of Geochemical Exploration*, 51(2), 109–130.

[21] Afzal, P., Alghalandis, Y. F., Khakzad, A., Moarefvand, P., & Omran, N. R. (2011). Delineation of mineralization zones in porphyry Cu deposits by fractal concentration-volume modeling. *Journal of Geochemical Exploration*, 108(3), 220–232.

[22] Ahmadi, H. and Uygucgil, H. (2021) Targeting Iron Prospective within the Kabul Block (SE Afghanistan) via Hydrothermal Alteration Mapping Using Remote Sensing Techniques. *Arabian Journal of Geosciences*, 14, Article No. 183.

[23] Hdeid, O. M., Morsli, Y., Raji, M., Baroudi, Z., Adjour, M., Nebagha, K. C., & Vall, I. B. (2024). Application of Remote Sensing and GIS in Mineral Alteration Mapping and Lineament Extraction Case of Oudiane Elkharoub (Requibat Shield, Northern of Mauritania). *Open Journal of Geology*, 14(9), 823–854.

[24] Chen, L., Sui, X., Liu, R., Chen, H., Li, Y., Zhang, X., & Chen, H. (2023). Mapping alteration minerals using ZY-1 02D hyperspectral remote sensing data in coalbed methane enrichment areas. *Remote Sensing*, 15(14), 3590.

[25] Wu, C., Dai, J., Zhou, A., He, L., Tian, B., Lin, W., & Bai, L. (2023). Mapping alteration zones in the Southern section of Yulong copper belt, Tibet using multi-source remote sensing data. *Frontiers in Earth Science*, 11, 1164131.

[26] Khademian, F., Alaminia, Z., Nadimi, A., Lentz, D. R., Ghasemi, A., & Sharifi, M. (2024). Structural and alteration zones controls on Cu mineralisation in the northwest of Nain (northeastern Isfahan, Iran): A remote sensing perspective. *Journal of African Earth Sciences*, 211, 105151.

[27] Alavi, M. (1980). Tectonostratigraphic evolution of the Zagrosides of Iran. *Geology*, 8(3), 144–149.

[28] Alavi, M. (1994). Tectonics of the Zagros orogenic belt of Iran: new data and interpretations. *Tectonophysics*, 229(3–4), 211–238.

[29] Berberian, M., & King, G. C. P. (1981). Towards a paleogeography and tectonic evolution of Iran. *Canadian journal of earth sciences*, 18(2), 210–265.

[30] Berberian, F., Muir, I. D., Pankhurst, R. J., & Berberian, M. (1982). Late Cretaceous and early Miocene Andean-type plutonic activity in northern Makran and Central Iran. *Journal of the Geological Society*, 139(5), 605–614.

[31] Rowan, L. C., Hook, S. J., Abrams, M. J., & Mars, J. C. (2003). Mapping hydrothermally altered rocks at Cuprite, Nevada, using the Advanced Spaceborne Thermal Emission and Reflection Radiometer (ASTER), a new satellite-imaging system. *Economic Geology*, 98(5), 1019–1027.

[32] Clark, R. N., King, T. V., Klejwa, M., Swayze, G. A., & Vergo, N. (1990). High spectral resolution reflectance spectroscopy of minerals. *Journal of Geophysical Research: Solid Earth*, 95(B8), 12653–12680.

[33] Kruse FA, Lefkoff AB, Boardman JB, Heidebrecht KB, Shapiro AT, Barloon PJ, Goetz A.F.H (1993) The Spectral Image Processing System (SIPS) – interactive visualization and analysis of imagingspectrometer data, *Remote Sensing of Environment* 44: 145–163.

[34] Tangestani MH, Mazhari N, Agar B, Moore F (2008) Evaluating Advanced Spaceborne Thermal Emission and Reflection Radiometer (ASTER) data for alteration zone enhancement in a semi-arid area, northern Shahr-e-Babak, SE Iran, *International Journal of Remote Sensing* 29: 2833-2850.

[35] Habashi, J., Moghadam, H. J., Oskouei, M. M., Pour, A. B., & Hashim, M. (2024). PRISMA hyperspectral remote sensing data for mapping alteration minerals in sar-e-châh-e-shur region, birjand, Iran. *Remote Sensing*, 16(7), 1277.

[36] Rossi, C., & Gholizadeh, H. (2023). Uncovering the hidden: Leveraging sub-pixel spectral diversity to estimate plant diversity from space. *Remote Sensing of Environment*, 296, 113734.

[37] Khojastehfar, S. , Ranjbar, H. and Shafiei Bafti, S. (2023). Sub-pixel Mineral Mapping of Serpentine and Magnesite for Chromite Exploration, Using Hyperion (EO1) Images. *Journal of Analytical and Numerical Methods in Mining Engineering*, 13(35), 39-49. doi: [10.22034/anm.2023.18911.1565](https://doi.org/10.22034/anm.2023.18911.1565)

[38] Ilyati, I. , Amanian, N. , Ansari, A. and Mokhtari, M. H. (2020). Combination of Remote Sensing and Ground Penetrating Radar methods to estimate suitable areas for locating subsurface dams in Abouzeidabad Plain. *Journal of Analytical and Numerical Methods in Mining Engineering*, 10(25), 1-11. doi: [10.29252/anm.2020.13980.1443](https://doi.org/10.29252/anm.2020.13980.1443)

[39] Mokhtari, Z. and Seifi, A. (2021). Detection of Hydrothermal Alteration Zones Using ASTER Remote Sensing Data in Turquoise mine of Neyshabur. *Journal of Analytical and Numerical Methods in Mining Engineering*, 11(28), 1-22. doi: [10.22034/anm.2021.203](https://doi.org/10.22034/anm.2021.203)